

Article

The Impact of Microclimate on the Reproductive Phenology of Female *Populus tomentosa* in a Micro-Scale Urban Green Space in Beijing

Xiaoyi Xing^{1,2,3} , Li Dong^{1,2,3,*}, Cecil Konijnendijk⁴ , Peiyao Hao^{1,2,3}, Shuxin Fan^{1,2,3} and Wei Niu¹

¹ School of Landscape Architecture, Beijing Forestry University, Beijing 100083, China; xiaoyixing1993@gmail.com (X.X.); peiyao hao@gmail.com (P.H.); fanshuxin_09@bjfu.edu.cn (S.F.); niuwei_bjfu_2019@163.com (W.N.)

² Laboratory of Beijing Urban and Rural Ecological Environment, Beijing Forestry University, Beijing 100083, China

³ National Engineering Research Center for Floriculture, Beijing Forestry University, Beijing 100083, China

⁴ Department of Forest Resources Management, The University of British Columbia, Vancouver, BC V6T 1Z4, Canada; cecil.konijnendijk@ubc.ca

* Correspondence: dongli@bjfu.edu.cn

Abstract: The spatial variation of poplars' reproductive phenology in Beijing's urban area has aggravated the threat of poplar fluff (cotton-like flying seeds) to public health. This research explored the impact of microclimate conditions on the reproductive phenology of female *Populus tomentosa* in Taoranting Park, a micro-scale green space in Beijing (range <1 km). The observed phenophases covered flowering, fruiting, and seed dispersal, and ENVI-MET was applied to simulate the effect of the microclimate on SGS (start day of the growing season). The results showed that a significant spatial variation in poplar reproductive phenology existed at the research site. The variation was significantly affected by the microclimate factors DMT (daily mean temperature) and DMH (daily mean heat transfer coefficient), with air temperature playing a primary role. Specifically, the phenology of flowering and fruiting phenophases (BBB, BF, FF, FS) was negatively correlated with DMT ($-0.983 \leq r \leq -0.908$, $p < 0.01$) and positively correlated with DMH ($0.769 \leq r \leq 0.864$, $p < 0.05$). In contrast, DSD (duration of seed dispersal) showed a positive correlation with DMT ($r = 0.946$, $p < 0.01$) and a negative correlation with DMH ($r = -0.922$, $p < 0.01$). Based on the findings, the increase in air convection with lower air temperature and decrease in microclimate variation in green space can be an effective way to shorten the seed-flying duration to tackle poplar fluff pollution in Beijing's early spring.

Keywords: ENVI-MET simulation; microclimate; micro-scale space; *Populus tomentosa*; reproductive phenology; spatial variation



Citation: Xing, X.; Dong, L.; Konijnendijk, C.; Hao, P.; Fan, S.; Niu, W. The Impact of Microclimate on the Reproductive Phenology of Female *Populus tomentosa* in a Micro-Scale Urban Green Space in Beijing. *Sustainability* **2021**, *13*, 3518. <https://doi.org/10.3390/su13063518>

Academic Editor: Åsa Gren

Received: 31 December 2020

Accepted: 23 February 2021

Published: 22 March 2021

Publisher's Note: MDPI stays neutral with regard to jurisdictional claims in published maps and institutional affiliations.



Copyright: © 2021 by the authors. Licensee MDPI, Basel, Switzerland. This article is an open access article distributed under the terms and conditions of the Creative Commons Attribution (CC BY) license (<https://creativecommons.org/licenses/by/4.0/>).

1. Introduction

The rapid changes in urban environments driven by the massive landscape reshaping during urbanization have dramatically shifted the growth rhythm of city plants [1–4]. The variation of the phenological temporal pattern can affect public health by influencing the occurrence period of phenology-triggered diseases [5,6].

A long-term phenology-correlated public health problem in Beijing is the seasonal respiratory diseases caused by the cotton-like flying seeds from *Populus tomentosa* (Chinese white poplar) and other Salicaceae species in early spring [7,8]. *P. tomentosa* is one of the most common and widespread deciduous woody species native to Beijing. It is dioecious and wind-pollinated, blooming in early spring before leafing [9]. In the 1960s, 0.2 million cloned female poplars were planted in Beijing city in a large-scale city greening action, in consideration of their rapid propagation and fast growth at a young age. Since then, the catkin fibers have become a major trigger of respiratory ailments, skin anaphylaxis,

inflammation, and other diseases in Beijing's early spring, posing a great risk to public health [10,11]. Beyond China, some other countries also face similar health problems caused by poplar fluff. For example, in Kashmir, India, the flying seeds of introduced Eastern Cottonwood (*Populus deltoides*) have given significant rise to the respiratory disease cases of local people in recent years [12,13]. In Abbottabad, Pakistan, as one of the main triggers of allergic asthma in spring, poplar fluff has caused severe psychological stress [14]. In Beijing, several strategies have been put forward by the Beijing Gardening and Greening Bureau to control poplar seed pollution, such as breeding sterile triploid female poplars, replacing female plants with male ones, and inhibiting catkin formation [15,16]. However, the heavy workload, high economic cost, and limited budget for treating such a huge number of targeted poplars made the implementation very difficult. Furthermore, the interindividual difference in the seed dispersal time between different regions or within green spaces extended the overall flying-seed period in Beijing's urban area [17], aggravating the threat of catkin fibers to public health. A profound understanding of the temporal pattern of poplars' reproductive phenology and the impact mechanism behind the spatial variation is the basic step to tackle this problem.

In recent years, a prominent intra-urban spatial variation of plant spring phenology has been found in many metropolises at both an urban scale (<50 km) [18–21] and micro-scale (<1 km) [19]. With regard to the impact mechanism associated with the intra-urban phenological variation, most of the research was conducted at an urban scale, revealing that the urban-scale variation in spring phenology was mainly driven by environmental factors, especially the near-surface air temperature that indicates urban heat [19,21,22]. However, the key influential factors of the phenological variation at the micro-scale are still largely unknown, even though a spatially uneven microclimate has been found in urban green spaces [23,24]. For urban-scale research, a significant phenological variation within a green space can affect the overall spatial pattern of studied phenology [22]. Therefore, more micro-scale studies need to be done.

In this research, we focused on the spatial variation of the reproductive phenology of female *P. tomentosa* in Taoranting Park, a micro-scale green space in Beijing, aiming to explore the key influential factors of this phenological variation. We attempted to answer two questions: (1) Is there a significant spatial variation in the reproductive phenology of female *P. tomentosa* in Taoranting Park? (2) What are the key influential factors for this variation? Assuming the impact mechanism at the micro-scale is similar to what has been widely revealed for the urban scale, we proposed two hypotheses to be tested.

Hypothesis 1 (H1): *There was no significant difference between the reproductive phenology of P. tomentosa in different sampling points of Taoranting Park ($p > 0.05$). H_1 : There was a significant difference between the reproductive phenology of P. tomentosa in different sampling points of Taoranting Park ($p < 0.05$).*

Hypothesis 2 (H2): *The spatial variation in reproductive phenology had no significant correlation with any microclimate factor ($p > 0.05$). H_1 : The spatial variation in reproductive phenology had a significant correlation with at least one of the microclimate factors ($p < 0.05$).*

Based on the revealed impact, this study attempted to gain some insight into more effective control and management of poplars' catkin fiber pollution in Beijing's early spring.

2. Materials and Methods

2.1. Research Site

The research was conducted in Taoranting Park, Xicheng District, Beijing, China. Beijing (39°54' N 116°24' E), the capital city of China, is located at the northern tip of the North China Plain. Beijing has a monsoon-influenced humid continental climate, characterized by hot, humid summers and cold, dry winters. Taoranting Park (39°52'21" N 116°22'32" E) is situated in the central downtown area of the dense capital city. As one of the

largest urban public gardens in Beijing, with a 65-year development history, Taoranting Park is famous for the flourishing vegetation with rich diversity and healthy growth conditions. The dense evergreen forest dominated by *Platycladus orientalis* (L.) and *Juniperus chinensis* L. together with deciduous groves has formed various green spaces in the garden, and the uneven landscape structure of the underlying surface has resulted in a highly diverse microclimate environment.

2.2. Research Object

Female *Populus tomentosa* (Chinese white poplar) trees growing in Taoranting Park were the research objects for phenological observation. According to the garden construction record, the adult female white poplars in Taoranting Park were planted in 1952. The seedlings were a batch of clones that were propagated with the cutting of root suckers from a stock plant. Therefore, the influence of genetic variation on the interindividual phenological variation [25,26] could be excluded in this research.

2.3. Selection of Sample Poplars and Setting of Sampling Points

There were eight female poplar populations distributed in the green space, with each population composed of 3–5 individuals. From each population, we selected two adjacent adult individuals with good growth conditions (that performed well in yearly growth and reproduction, with no sign of diseases or being subject to serious environmental stress) as the sample poplars of this population; their canopy height ranged from 5 to 11 m. The central growing point of the two sampling trees was set as the sampling point; the distribution of eight sampling points is shown in Figure 1.



Figure 1. The distribution of sampling points and setting of the buffer area in Taoranting Park. The background image is the Worldview-3 satellite image of Taoranting Park taken in February 2019.

From each sampled individual, three branchlets at the height of 7–9 m above ground were selected for phenological observation, with 20–30 catkins growing on each branchlet. A branchlet refers to a 2-year-old branch formed in the previous year [27]. The phenology data of each branchlet were obtained from the earliest catkin, and the data for each sampling point were the values of six branchlets (three branchlets/individual \times two individuals).

2.4. Setting of the Buffer Area

A buffer area was set around each sampling point for microclimate simulation. Each buffer area was a 100 m × 100 m square centered on the sampling point, as shown in Figure 1. The size of the buffer area was determined with reference to the findings of previous research, i.e., that the microclimate of a point in urban green land can interact with the thermal environment of its surrounding area within a range of 100–200 m [24,28,29]. Considering that the distance between any two sampling points was less than 100 m in this research, the side length of the square buffer area was set to 100 m to prevent considerable overlap.

2.5. Data Collection

2.5.1. Reproductive Phenology Data Collection

The reproductive phenology of female *P. tomentosa* was observed from February 20 until April 18 in 2019, covering the entire reproduction process from the beginning of bud break to the end of seed dispersal. The observation was conducted every day at 13:00–14:00, when the air temperature reaches its daily maximum and often drives a phenological change [30].

The BBCH (Biologische Bundesanstalt, Bundessortenamt and Chemical Industry) scale was used to identify the phenological development stages, i.e., phenophases [31], and the phenology data of each phenophase were recorded in Julian Day (the day of the year). The observed phenophases covered flowering, fruiting, and seed dispersal, including the Beginning of Bud Break (BBB, 07)—bud scales spread open with the catkin top visible, Beginning of Flowering (BF, 60)—the first few flowers bloom, Full Flowering (FF, 65)—more than 95% flowers bloom, Fruit Set Visible (FS, 69)—green fruits appear behind flowers, Beginning of Seed Dispersal (BSD, 89a)—pericarps crack and the first few seeds covered with white fibers detach, End of Seed Dispersal (ESD, 89b)—all the seeds detach from peduncles, and Duration of Seed Dispersal (DSD, N/A)—The period between BSD and ESD. The number in the parentheses is the BBCH code for each phenophase (Finn et al., 2007). The detailed images of the reproductive phenophases are shown in Figure 2.



Figure 2. Detailed images of the reproductive phenophases of female *P. tomentosa*. (a) Beginning of bud break (BBB), (b) Beginning of flowering (BF), (c) Full flowering (FF), (d) Fruit set visible (FS), (e) End of flowering, (f) Beginning of seed dispersal (BSD), (g) Peak of seed dispersal, (h) End of seed dispersal (ESD).

2.5.2. Data Collection of Microclimate Factors with ENVI-MET Simulation

We needed to evaluate the microclimate environment at the height of the sampled branches (7–9 m). Field data measurements are generally accepted and widely applied in the data collection of the microclimate condition, including using fixed equipment [32]. However, this method was not feasible in this research, subject to the management regulation of the Park Administrative Office, that no equipment was allowed to be attached to tree branches to prevent potential damage caused to the plants. Unable to measure the microclimate with field data, we applied ENVI-MET software (ENVI-MET 4.0, sourced from ENVI_met GmbH, Essen, Germany) for microclimate simulation in the micro-scale green space.

ENVI-MET is holistic, three-dimensional and non-hydrostatic modeling software, developed by the research team of Professor Michael Bruse at Johannes Gutenberg University Mainz [33]. Based on computational fluid dynamics, ENVI-MET is often used to simulate

urban microclimate environments and evaluate the effects of small-scale variations in urban design (e.g., atmosphere, vegetation, architecture, and materials) on the microclimate [34–40]. ENVI-MET has some functions in favor of phenological research. Firstly, the 3D modeling can simulate meteorological conditions at a specific height, a favorable point for the phenological research of tree species, whose reproductive phenology can be directly affected by the microclimate condition at canopy height via bud temperature perception [41]. Secondly, ENVI-MET can simulate multiple microclimate parameters, e.g., air temperature, convection, and wind, which can help explore the key microclimate factors that affect plant phenology. These characteristics provide evidence for its applicability in phenological research.

The microclimate simulation in ENVI-MET mainly includes the following several steps: (1) Create a Workspace in *Manage Projects and Workspaces*, (2) Construct a 3D model in *SPACES*, (3) Run the Simulation in *ENVIGuide*, (4) Extract data in *LEONARDO*.

3D Model Construction

The satellite images of the eight 100 m × 100 m buffer areas were extracted from the Worldview–3 image of Taoranting Park in February 2019 as the background image for model construction. A network of 50 grids (x) × 50 grids (y) × 30 grids (z) with a resolution ratio of 2 m/grid was constructed for each buffer area in ENVI-MET.

The basic model elements include architecture, vegetation, DEM (topography), soil, and surface (including water). The height of landscape elements (e.g., evergreen trees and architecture) was measured with Nikon Forestry Pro, i.e., laser rangefinder equipment. The height of the architecture and single trees was measured one by one, while the height of evergreen forest was measured using 3–5 sample trees at the forest edge surrounding the sampling point. The topography data were extracted from Google Earth Pro. The vegetation and architecture layer of the constructed models is shown in Figure 3, which can reflect the various landscape structures of the underlying surface of the eight buffer areas.

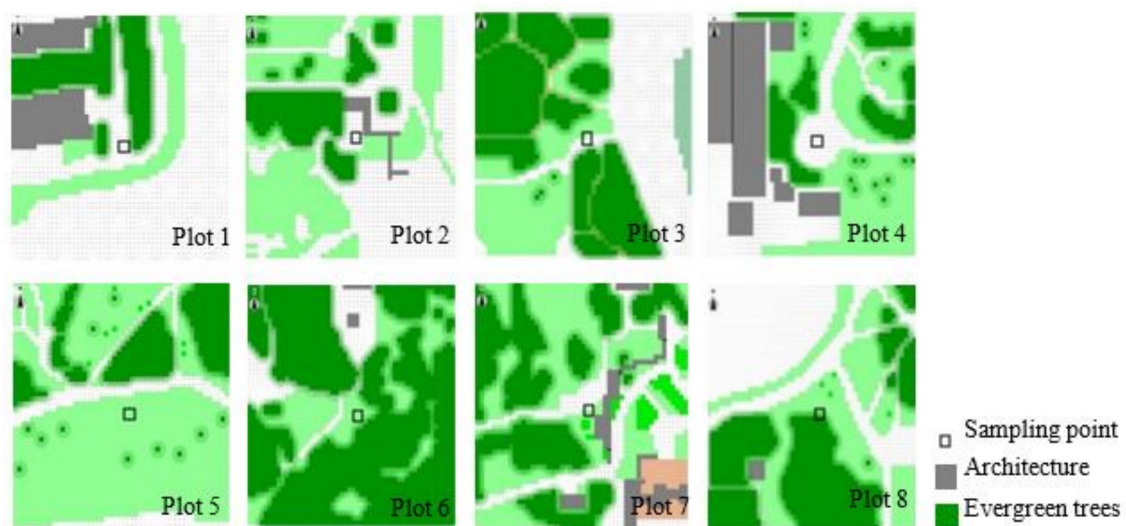


Figure 3. The vegetation and architecture layer of the ENVI-MET model for the eight buffer areas.

Microclimate Simulation

Simulation time. The number of days for microclimate simulation varied between different studies, ranging from one day [42,43] to three days [44] or more [33,45]. Generally, the simulation of the microclimate for each hour would take 0.5–1.5 h in ENVI-MET (when running on equipment with a Core i7 processor and 8 Gb RAM), which varied depending on the complexity of the models and the running speed of the equipment. In this research, the ENVI-MET simulation for one-day microclimate of the eight models (eight buffer areas) would take more than 10 days with tests and final running time taken into account.

Spring phenology in temperate zones is affected by the microclimate of the development period prior to the phenophase occurrence [46]; therefore, the microclimate during this period was expected to be simulated in this research. Considering the high time consumption of ENVI-MET simulation for the eight buffer areas, we chose to simulate the microclimate condition on 25 February 2019, the start of the growing season (SGS) for *P. tomentosa* in Beijing. SGS was chosen for simulation considering that the above-threshold air temperature at the onset of the growing season could be an effective stimulus to initiating spring phenology, such as sprouting and flowering [46]. SGS is defined as the beginning of the first six consecutive days with local daily mean air temperature $> 5\text{ }^{\circ}\text{C}$, the general threshold temperature for tree growth in temperate zones [47,48]. The date of SGS was calculated based on the dynamics of daily mean temperature in Beijing's early spring (shown in Appendix A, Figure A1). The simulation extended a period of 24 h from 0:00 to 24:00. Each simulation had been repeated twice before to ensure a steady running condition in the final round.

Initial meteorological condition preset. We preset the initial meteorological condition including wind, temperature, and humidity. We used min/max temperature bounds for forcing in ENVI-MET. The data for the meteorology preset came from the *Hourly Observation Dataset of Surface Meteorological Stations* in Beijing Station (54,511, 39°48' N, 116°28' E, 31.5 m elevation above sea level), retrieved from the Chinese Meteorological Data Network (<http://data.cma.cn/>) (accessed on 15 March 2021). The detailed setting of the background meteorological condition is shown in Table 1.

Table 1. The setting of background parameters for microclimate simulation in ENVI-MET.

Parameters	Wind Speed Measured at 10 m Height (m/s)	Wind Direction (deg)	Minimum Temperature of the Atmosphere ($^{\circ}\text{C}$)	Maximum Temperature of the Atmosphere ($^{\circ}\text{C}$)	Minimum Relative Humidity at 2 m (%)	Maximum Relative Humidity at 2 m (%)
Set value	1.89	45	−2	12	17	47

Simulation. The microclimate simulation was run in *ENVIGuide*. The output data were stored in SIMX files.

Data Extraction and Calculation of Microclimate Parameters

Data extraction. The output of the ENVI-MET simulation provided hourly data of multiple microclimate parameters. In this research, the air temperature ($^{\circ}\text{C}$), heat transfer coefficient (m^2/s), and wind speed (m/s) were selected as the microclimate factors to be analyzed. The heat transfer coefficient/heat exchange coefficient is a proportionality constant between the heat flux and the thermodynamic driving force for the flow of heat [49]. In thermodynamics, the heat transfer coefficient usually indicates the overall heat transfer rate, reflecting the efficiency and activeness of air convection, and is considerably affected by the pattern of air-flow and the geometry of solid space [49,50]. In this study, besides the two basic factors, air temperature and wind speed, the heat transfer coefficient was also used to explore the impact of convection efficiency on reproductive phenology.

Calculation of microclimate parameters. Considering that the reproductive phenology of sampling branchlets could be directly affected by the surrounding microclimate condition, the microclimate data of each sampling point was extracted from the central eight grids in the 4 m (x -axis) \times 4 m (y -axis) \times 2 m (h -axis) model space. The 4 m \times 4 m horizontal area was constituted by four grids (25,25),(25,26),(26,25),(26,26) at each height, the vertical range of 2 m covered the height of 7 m and 9 m (the height of sampled branchlets). The values of the daily mean air temperature (DMT), daily mean heat transfer coefficient (DMH), and daily mean wind speed (DMW) for each grid were calculated with the hourly

simulated data. Taking air temperature as an example, the DMT for each sampling point was calculated with Formula (1).

$$\overline{DMT}_n = \frac{\sum_{x=25,26} \sum_{y=25,26} \sum_{h=7,9} (DMT_n)_{xyh}}{4 * 2}, \quad n = 1, 2, 3 \dots \dots 8 \quad (1)$$

where \overline{DMT}_n refers to the DMT of sampling point n ; x, y, h refer to the respective x -ordinate, y -ordinate, and h -ordinate of a grid in the model; $(DMT_n)_{xyh}$ refers to the DMT on the grid (x, y, h) of sampling point n .

The Accuracy Evaluation of ENVI-MET Microclimate Simulation

The measured and simulated air temperature 1.5 m above ground was used for the accuracy evaluation. The air temperature of 1.5 m above ground (T_a) is one of the standard indexes for the performance evaluation of ENVI-MET microclimate simulation [39,51,52]. The field data of air temperature at eight sampling points were simultaneously collected at 9 a.m., 11 a.m., and 13 p.m. on February 25, with TES–1314, a high-accuracy handheld digital hygrometograph.

A suite of quantitative indices for model evaluation recommended by Willmott (1982) [53], was used to evaluate the model performance, including the root mean square error ($RMSE$), systematic errors ($RMSE_s$), unsystematic errors ($RMSE_u$), and the index of agreement (d). With a purpose to obtain an accurate simulation outcome, the magnitude of $RMSE_s$ should approach 0, the value of $RMSE_u$ should approach $RMSE$, and the value of d should approach 1. $RMSE$, $RMSE_s$, $RMSE_u$, and d were calculated with Formulas (2)–(8) [54,55].

$$RMSE = \sqrt{RMSE_s^2 + RMSE_u^2} \quad (2)$$

$$RMSE_s = \sqrt{N^{-1} \sum_{i=1}^N (\hat{P}_i - O_i)^2} \quad (3)$$

$$RMSE_u = \sqrt{N^{-1} \sum_{i=1}^N (P_i - \hat{P}_i)^2} \quad (4)$$

$$\hat{P}_i = f(O_i) = E(O_i|P_i) = a + bO_i \quad (5)$$

$$d = 1 - \left[\frac{\sum_{i=1}^N (P_i - O_i)^2}{\sum_{i=1}^N (|P'_i| + |O'_i|)^2} \right], 0 \leq d \leq 1 \quad (6)$$

$$P'_i = P_i - \bar{O} \quad (7)$$

$$O'_i = O_i - \bar{O} \quad (8)$$

where O_i refers to the observed value, P_i refers to the simulated value, \hat{P}_i refers to the fitted value from the linear regression equation between the observed value and simulated value, and \bar{O} refers to the average of observed values.

2.6. Statistical Analysis

2.6.1. MANOVA (Multivariate Analysis of Variance) of the Reproductive Phenology among Different Sampling Points

Multivariate analysis of variance (MANOVA) was applied to explore whether there was a significant variation in the reproductive phenology of female *P. tomentosa* among the eight sampling points within the green space. The dependent variables for MANOVA included the phenology of various reproductive phenophases—BBB (beginning of bud break), BF (beginning of flowering), FF (full flowering), FS (fruit set visible), BSD (beginning of seed dispersal), ESD (end of seed dispersal), DSD (duration of seed dispersal).

2.6.2. Pearson Correlation Analysis between Reproductive Phenology and Microclimate Factors

Pearson correlation between the microclimate parameters and reproductive phenology was analyzed to explore the key microclimate factors that had a significant influence on the spatial variation of studied phenology and to reveal the quantitative impact. The independent variables for Pearson correlation analysis included DMT (daily mean temperature), DMH (daily mean heat transfer coefficient) and DMW (Daily mean wind speed); the analyzed dependent variables included the phenology of the reproductive phenophases—BBB, BF, FF, FS, BSD, ESD, DSD.

2.6.3. Multiple Regression Analysis of Reproductive Phenology in Relation to Multiple Microclimate Factors

Multiple regression analysis was performed to explore the overall correlation pattern between the phenology of each reproductive phenophase and multiple microclimate factors (DMT, DMH, DMW). According to the primary multiple regression analysis, there was a high-degree multicollinearity between DMT and DMH with VIF (variance inflation) >10. In response to the problem of multicollinearity, we applied Ridge Regression in the multiple regression analysis [56,57].

3. Results

3.1. Simulated Microclimate Conditions in Taoranting Park

With respect to the accuracy evaluation of the air temperature simulation in ENVI-MET, $RMSE = 1.057\text{ }^{\circ}\text{C}$, $RMSE_s = 0.684\text{ }^{\circ}\text{C}$, $RMSE_u = 0.806\text{ }^{\circ}\text{C}$, $d = 0.962$. With $RMSE_u$ approaching $RMSE$ and d approaching 1, the model performance can be evaluated as ‘good’, which means the ENVI-MET simulation could reflect the actual thermal environment in this research. The detailed data of the accuracy evaluation are shown in Appendix A, Table A1 and Figure A2.

Among the eight sampling points, DMT (daily mean temperature) ranged from 4.578 to 5.071 $^{\circ}\text{C}$, $SD = 0.147\text{ }^{\circ}\text{C}$; DMH (daily mean heat transfer coefficient) ranged from 0.440 to 1.403 m^2/s , $SD = 0.300\text{ m}^2/\text{s}$; DMW (daily mean wind speed) ranged from 0.017 to 0.160 m/s , $SD = 0.079\text{ m}/\text{s}$. A significant correlation was found between DMT and DMH ($r = -0.920$, $p < 0.01$), which means a higher air temperature was associated with a lower convection rate. The simulated data of the microclimate factors are shown in Appendix A, Table A2.

3.2. Spatial Variation of the Reproductive Phenology of Female *P. tomentosa* in Taoranting Park

The multivariate tests (MANOVA) showed that there was a statistically significant difference in the phenology of analyzed reproductive phenophases among the eight sampling points ($p < 0.01$). As seen in Figure 4, the phenology of BBB showed the most significant spatial difference, and the between-point phenological variation in flowering phenophases (BF, FF) was more significant than that in the fruiting and seed dispersal phenophases (FS, BSD).

In the micro-scale green space, the entire reproduction process of female *P. tomentosa* occurred from Julian day 58 (27 February)–Julian day 106 (16 April), from the earliest flower bud breaking to the latest time of seed dispersal. The beginning of bud break (BBB) ranged from Julian day 58 to day 63, the beginning of flowering (BF) ranged from day 65 to day 71, full flowering (FF) ranged from day 67 to day 72, fruit set visible (FS) ranged from day 70 to day 73, beginning of seed dispersal (BSD) ranged from day 93 to day 96, end of seed dispersal (ESD) ranged from day 102 to day 106, and duration of seed dispersal (DSD) ranged from 6 days to 12 days.

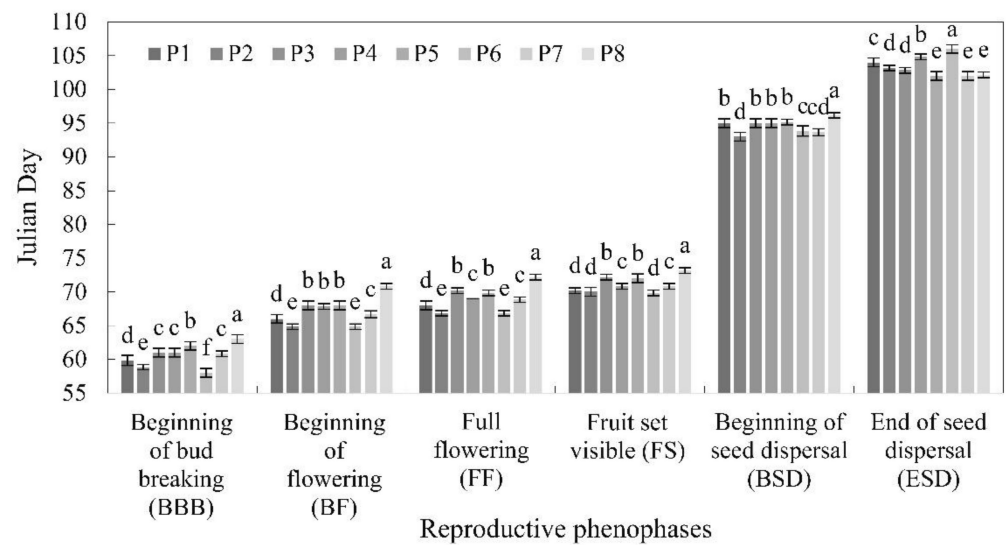


Figure 4. The reproductive phenology of female *P. tomentosa* at eight sampling points.

A significant positive correlation was found between BBB, BF, FF, FS, BSD, the phenophases at flowering and fruiting stage ($0.781 \leq r \leq 0.986$, $p < 0.05$), while they showed a significantly negative correlation with DSD ($-0.930 \leq r \leq -0.840$, $p < 0.01$). This contrast indicated that the seed dispersal of female *P. tomentosa* could be a different process inconsistent with the flowering and fruiting development. The raw phenology data are presented in Appendix A, Table A3.

3.3. Key Microclimate Factors Affecting the Reproductive Phenology of Female *P. tomentosa* in Taoranting Park

According to the Pearson correlation analysis between reproductive phenology and the daily mean value of three microclimate parameters associated with SGS, we found that the phenology of the reproductive phenophases was heavily dependent on air temperature and the heat transfer coefficient, while wind speed showed no significant correlation.

3.3.1. Air Temperature vs. Reproductive Phenology

As shown in Figure 5, the DMT (daily mean temperature) associated with SGS was significantly negatively correlated with the phenology of BBB, BF, FF, FS, BSD, which means a higher air temperature at the onset of the growing season could drive an earlier occurrence of flowering and fruiting in female *P. tomentosa*. For BBB, BF, FF, and FS that happened successively within 15 days from the beginning of reproduction, the correlation was extremely significant ($-0.983 \leq r \leq -0.908$, $p < 0.01$), while the phenology of BSD that happened over 20 days after the appearance of fruit set showed a weaker correlation with DMT ($r = -0.754$, $p < 0.05$). Besides, according to the linear regression analysis, the absolute slope of the regression decreased with the occurrence time of the phenophases, with a change rate of -12.64 day/ $^{\circ}\text{C}$ for BF to -5.23 days/ $^{\circ}\text{C}$ for BSD. This difference demonstrated that the 'driving effect' of the air temperature at the onset of the growing season could become weaker for those phenophases occurring at later reproduction stages.

With respect to ESD and DSD, the correlation pattern reversed. Their positive correlation with DMT ($r = 0.749$, $p < 0.05$; $r = 0.946$, $p < 0.01$) indicated a different impact mechanism behind the seed dispersal process.

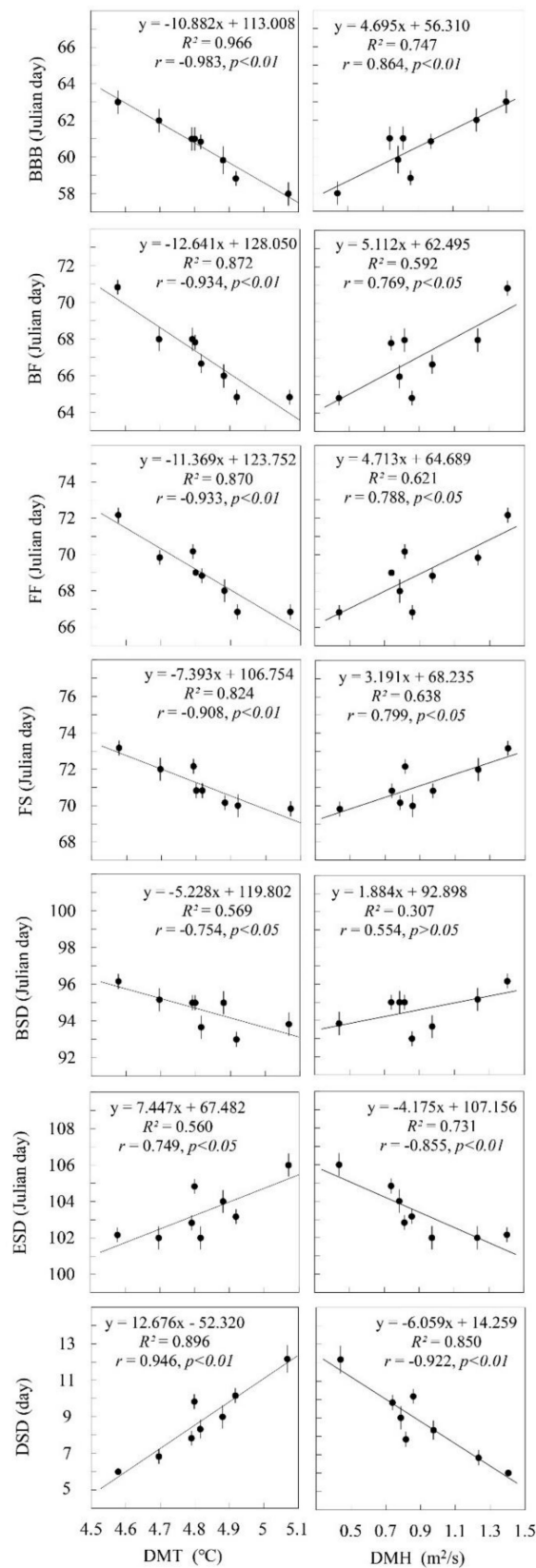


Figure 5. The correlation between microclimate factors (DMT, DMH on SGS) and the reproductive phenology of female *P. tomentosa*. DMT—daily mean temperature, DMH—daily mean heat transfer coefficient, BBB – beginning of bud break, BF—beginning of flowering, FF—full flowering, FS—fruit set visible, BSD—beginning of seed dispersal, ESD—end of seed dispersal, DSD—duration of seed dispersal.

3.3.2. Heat Transfer Coefficient vs. Reproductive Phenology

As shown in Figure 5, the DMH (daily mean heat transfer coefficient) associated with SGS was significantly positively correlated with BBB ($r = 0.864$, $p < 0.01$), BF ($r = 0.769$, $p < 0.05$), FF ($r = 0.788$, $p < 0.05$), and FS ($r = 0.799$, $p < 0.05$). The positive correlation means a lower air convection rate could advance the occurrence of flowering and fruiting phenophases, especially in the early development stage. According to the linear regression between phenology and DMH, the slope of the regression decreased with the phenophase occurrence time, from 5.11 day/(m²/s) for BF to 1.88 day/(m²/s) for BSD, which indicated a declining influence of the heat transfer coefficient at SGS on the late-occurring phenophases. In addition, similar to DMT, the correlation between DMH and phenology ceased to be negative with respect to DSD ($r = -0.922$, $p < 0.01$).

Compared with air temperature, the heat transfer coefficient had a less significant impact on the reproductive phenology, reflecting on a lower absolute r (correlation coefficient) for most analyzed phenophases.

3.4. Multiple Regression of Reproductive Phenology in Relation to Microclimate Factors

Based on Ridge Regression analysis, the regression models of the phenology for various reproductive phenophases (BBB, BF, FF, FS, BSD and DSD) are shown as follows.

$$\begin{aligned}
 D_{BBB} &= 96.230 - 7.781 X_{DMT}^{**} + 1.607 X_{DMH}^* + 4.797 X_{DMW} \quad (R^2 = 0.962, p < 0.01, k = 0.1) \\
 D_{BF} &= 120.203 - 11.257 X_{DMT}^* + 0.744 X_{DMH} + 6.335 X_{DMW} \quad (R^2 = 0.887, p < 0.05, k = 0.08) \\
 D_{FF} &= 120.381 - 10.759 X_{DMT}^* + 0.213 X_{DMH} + 3.025 X_{DMW} \quad (R^2 = 0.875, p < 0.05, k = 0.06) \\
 D_{FS} &= 104.534 - 6.942 X_{DMT}^* + 0.055 X_{DMH} \quad (R^2 = 0.821, p < 0.05, k = 0.05) \\
 D_{BSD} &= 110.402 - 3.816 X_{DMT} + 1.731 X_{DMH} + 13.010 X_{DMW} \quad (R^2 = 0.843, p < 0.05, k = 0.01) \\
 D_{DSD} &= -23.747 + 7.255 X_{DMT}^* - 2.658 X_{DMH}^* - 0.489 X_{DMW} \quad (R^2 = 0.911, p < 0.05, k = 0.07)
 \end{aligned}$$

where D refers to the phenology (Julian day) or duration (days) of phenophases; X_{DMT} refers to the value of the daily mean temperature at SGS, X_{DMH} refers to the value of the daily mean heat transfer coefficient at SGS, X_{DMW} refers to the value of the daily mean wind speed at SGS; k refers to the ridge parameter; * refers to the factor that had a significant influence on the analyzed phenology in the ridge regression model (* $p < 0.05$, ** $p < 0.01$).

In general, the regression models for various phenophases showed a satisfactory fit ($\overline{R^2} = 0.883$, $p < 0.05$) especially for BBB and DSD, which means the three microclimate factors could explain more than 88% of the spatial variation in reproductive phenology. In the regression of flowering and fruiting phenophases, BBB, BF, FF, FS, and DMT had a significantly negative influence on the phenology, while DMH showed a weaker positive correlation. As regards to the regression of DSD, the correlation pattern shifted, where DMT exerted a significantly positive impact on seed dispersal duration while DMH showed a negative effect.

4. Discussion

4.1. Testing of Hypothesis 1: There Was a Significant Difference between the Reproductive Phenology of *P. tomentosa* at Different Sampling Points in Taoranting Park (H_1)

H_1 was true based on the MANOVA results, i.e., that the phenology of the analyzed reproductive phenophases all showed a statistically significant difference among the eight sampling points ($p < 0.05$). This is consistent with the finding that a significant spatial unevenness of plant phenology could appear in a small-scale urban space [19] or natural space [58–60]. Affected by this spatial variation, the duration of seed dispersal for female *P. tomentosa* in the green space extended from the average of 8.8 days for an individual to 13 days in total, aggravating the threat of poplar fluff to public health, let alone the impact at the urban scale, which highlights the need for more micro-scale studies in this field.

4.2. Testing of Hypothesis 2: The Spatial Variation of Reproductive Phenology Had a Significant Correlation with at Least One of the Microclimate Factors (H_1)

H_1 was true based on the results of the correlation and regression analyses, i.e., that the DMT and DMH at SGS were significantly correlated with the reproductive phenology of female *P. tomentosa* ($p < 0.05$). Besides, air temperature played a key role in the multiple regression of reproductive phenology for various phenophases, showing a more significant impact on phenology than other factors. This also illustrated that in the studied garden area, the primary influence on poplar's reproductive phenology was air temperature, and other microclimate factors might exert their effects by affecting or interacting with temperature.

This significant correlation showed that a slight microclimate variation could lead to an obvious spatial unevenness of reproductive phenology in such a micro-scale green space.

4.2.1. Air Temperature

The significant linear correlation between the air temperature and phenology of the reproductive phenophases demonstrated the prominent influence of the micro-scale thermal environment on poplar's reproductive development in Beijing's early spring. This finding accords with the widely accepted conclusion that air temperature is the critical climate driver of spring flowering and sprouting phenology in temperate zones [60–64], including poplar's reproduction [65].

The simulated air temperature at SGS performed well in the correlation and regression analyses, but the limitation of the one-day simulated data should be mentioned as well. In this research, the R^2 (coefficient of determination) of the linear regression between air temperature and phenology decreased as the phenophases occurred later, which means the ability of the temperature data at SGS to explain the spatial variation in late-occurring phenophases (e.g., FS, BSD) declined. Some studies revealed that multi-day thermal accumulation, e.g., Growing Degree Days, is the decisive initiator of spring phenology and has been widely applied in phenology modeling [66,67]. From this perspective, the one-day simulated microclimate data may not be robust enough for phenology prediction, and multi-day data simulation or observation is needed in future research.

4.2.2. Heat Transfer Coefficient

In addition to air temperature, the heat transfer coefficient was also found to have a significant impact on the reproductive phenology of female poplars. In Beijing in late February, a much lower heat transfer coefficient in an urban microclimate usually indicates a less frequent air disturbance from the outer cold airflow (e.g., Skimming flow regime), which is conducive to the establishment of a stable flow pattern with independent circulatory vortexes and a steady thermal field [49] that can provide a favorable condition for reproductive development. As a micro-scale parameter, the role of the heat transfer coefficient in affecting phenological variation was rarely explored before and deserves more attention.

4.2.3. Wind Speed

As an important impact factor of air temperature [68,69] and the heat transfer coefficient [70] in urban microclimates, wind speed is expected to show a clear correlation with the studied phenology. However, in this research, the correlation between wind speed and the phenology of reproductive phenophases was not significant, even though wind speed had a weak positive impact on the flowering and fruiting phenophases and a negative influence on the duration of seed dispersal in the multiple regression models.

One possible reason for this discrepancy could be the poor simulation accuracy of wind speed in ENVI-MET. Due to the lack of measurement data for comparison and validation, the performance of wind simulation could not be evaluated in this research. A challenge in the wind simulation is due to the unique wind environment in the micro-scale green space. Different from open urban spaces characterized with strong wind fields (e.g., urban canyons) [71], the large area of evergreen woods in the research site

could function as a wind obstacle, decreasing the turbulence of high-momentum fluid [72], forming small vortexes with changeable airflow [73]. Further, the weak wind field in Beijing city on the simulated day (1.89 m/s at 10 m height), the changeable wind pattern, and low wind speed could bring a large challenge to the wind simulation in ENVI-MET [74,75].

The unexpected correlation pattern between wind speed and reproductive phenology showed the limitation of ENVI-MET in wind environment simulation, highlighting the need for field data as a support.

4.3. Some Insights into the Alleviation of Catkin Fiber Pollution from Female Poplars

Based on the revealed impact of microclimate factors on the reproductive phenology of female *P. tomentosa*, some potential strategies to alleviate the catkin fiber pollution can be proposed.

(1) Shorten the seed-flying period by increasing air convection and decreasing spatial variation of the microclimate in the green space.

The phenological response of seed dispersal to microclimate factors showed that the duration of seed dispersal (DSD) was significantly correlated with air temperature ($r = 0.946$) and the heat transfer coefficient ($r = -0.922$). Considering the heat transfer coefficient, the indicator of air convection, has been proved to be positively correlated with the spatial openness [49], to improve the air convection by increasing spatial openness can be an effective way to shorten the duration of seed dispersal for each individual poplar. In addition, the decrease in microclimate variation in the green space can help standardize the thermal environment around target trees and reduce the spatial variation of reproductive phenology, so as to shorten the overall duration of seed dispersal. Of course, the implementation of this potential strategy can be subject to reality and a comprehensive trade-off consideration, which deserves further discussion.

(2) Time arrangement of flying seed control based on the phenological response to air temperature.

According to the linear regression, with an increase in the daily mean temperature at SGS of 1 °C, BSD could advance 5.23 days and DSD could extend over 10 days. Combining local meteorological data, the phenological response of seed dispersal to air temperature variation can provide a reference to the timing of flying-seed control in Beijing's different urban heat environments (Yang et al., 2013).

4.4. Research Prospect—Other Possible Influential Factors Besides the Microclimate?

As shown in Figure 4, among the eight sampling points, the female *P. tomentosa* at point 8 showed a significantly later phenology than at other points for most analyzed phenophases (BBB, BF, FF, FS, BSD), and the poplars at points 2 and 6 showed a significantly earlier phenology than that at other points. According to the landscape pattern of the eight buffer areas shown in Figure 3, point 8 was situated in a highly open space with a wide wind corridor, while points 2 and point 6 were highly enclosed by evergreen groves. This indicates a possible correlation between the spatial structure (e.g., spatial openness) and reproductive phenology. Besides, the spatial structure of the underlying surface has been proved to have a significant influence on the air temperature in urban microclimates [24,49,76]. Therefore, a possible impact mechanism of the spatial structure—microclimate—reproductive phenology should be explored in follow-up research.

5. Conclusions

This research investigated the impact of microclimate factors on SGS (start of the growing season) on the spatial variation in the reproductive phenology of *P. tomentosa* in a micro-scale green space in Beijing. We found that the phenology of the flowering and fruiting phenophases of female poplars was significantly negatively correlated with DMT (daily mean temperature) and positively correlated with DMH (daily mean heat transfer coefficient), while the duration of seed dispersal was positively affected by DMT and negatively affected by DMH. Based on the findings, an increase in air convection

with lower air temperature and a decrease in the spatial variation of microclimates in green spaces can be an effective way to shorten the seed-flying duration, so as to help tackle poplar's catkin fiber pollution in Beijing. The discovery of this research can help fill the knowledge gap in the impact mechanism of the microclimate with respect to plant phenology in a micro-scale urban green space. It can also provide some empirical guidance for the alleviation of catkin fiber pollution in Beijing and other countries facing a similar problem.

Meanwhile, some limitations of this research need to be noted. ENVI-MET microclimate simulation (especially thermal environment simulation) was suitable for this phenological study, but field data measurements are still strongly advocated for the data collection for microclimate conditions to ensure data accuracy. Subject to the management regulation of the Park Administrative Office, we were unable to collect microclimate data with field measurements in this research. Regarding this, we will try to improve the access to field data in our future work. Another limitation was that the one-day simulated microclimate was not robust enough for phenology prediction, which addressed the importance of multi-day data collection in follow-up work.

Author Contributions: Conceptualization, X.X., L.D., C.K.; Funding acquisition, L.D.; Project administration, L.D.; Data acquisition, X.X., W.N., Formal analysis, X.X., P.H., S.F.; Drafting the manuscript, X.X., L.D., C.K.; Revising the manuscript critically for important intellectual content, X.X., L.D., C.K. All authors have read and agreed to the published version of the manuscript.

Funding: This study was funded by the Beijing Municipal Science and Technology Commission (D171100007117001).

Institutional Review Board Statement: Not applicable.

Informed Consent Statement: Not applicable.

Data Availability Statement: Data is contained within the article.

Acknowledgments: This research was funded by Beijing Municipal Science and Technology Project: Establishing Evaluation System for Ecological Function of Multi-scale Green Spaces in the Northern Urban Area (D171100007117001) and was supported by The Study on the Plant Resources Collection, Rapid Propagation, and Applied Technology of Fine Species with Richer Coloration and Prolonged Green Period in Beijing Urban Greening (CEG2018). We would like to thank Sijia Wu, Yilun Li, Kun Li and Mengyuan Zhang for their support in the field work and research methods. We sincerely thank the anonymous reviewers for their valuable comments.

Conflicts of Interest: The authors declare no conflict of interest.

Appendix A

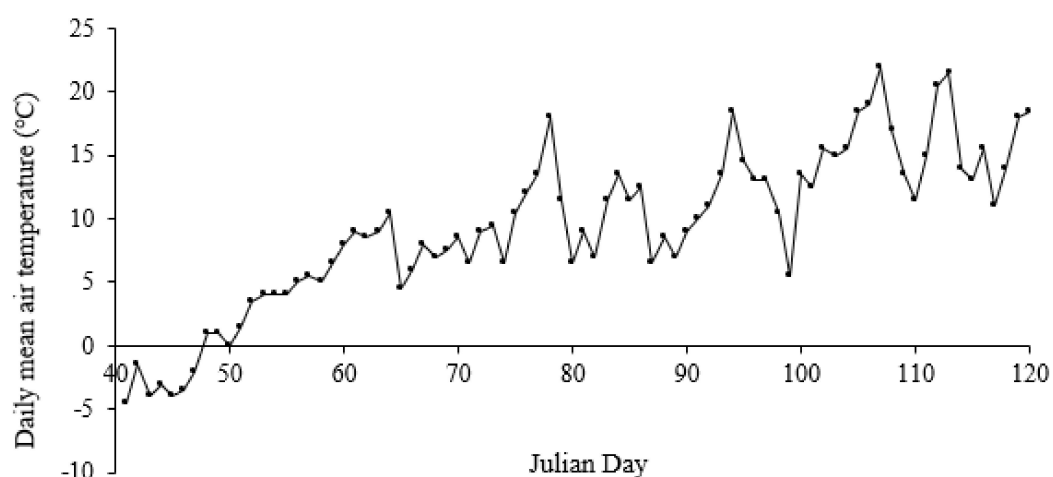


Figure A1. The Daily Mean Air Temperature of Beijing City in the Spring (10 February—30 April/Julian Day 41–120) of 2019. Data Came from the Hourly Observation Dataset of Surface Meteorological Stations in Beijing Station (54511).

Table A1. The Observed and Simulated Data for the Accuracy Evaluation of Air Temperature Simulation with ENVI-MET.

Sampling Point	Time/h	O (Observed Value)/°C	P (Simulated Value)/°C
1	9	7.900	7.359
1	11	10.200	9.891
1	13	10.700	11.938
2	9	9.100	7.521
2	11	11.300	10.204
2	13	11.500	12.050
3	9	8.900	7.088
3	11	10.000	9.599
3	13	11.300	11.655
4	9	7.300	7.162
4	11	11.700	10.077
4	13	12.300	12.449
5	9	9.200	7.454
5	11	11.000	10.207
5	13	12.200	12.322
6	9	8.400	7.243
6	11	10.400	9.742
6	13	13.500	11.999
7	9	8.700	7.467
7	11	10.000	10.184
7	13	12.600	12.128
8	9	9.100	6.955
8	11	9.900	9.234
8	13	11.600	11.257

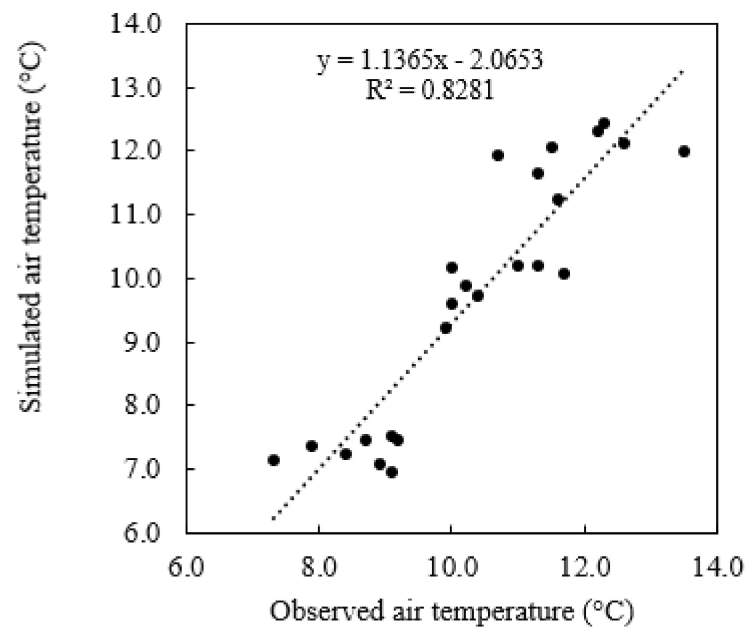
**Figure A2.** The linear regression between the observed and simulated air temperature at height of 1.5 m.

Table A2. The Simulated Values of Microclimate Parameters.

Sampling Point	Height/m	Grid	Air Temperature (°C)	Heat Transfer Coefficient (m ² /s)	Wind Speed (m/s)
1	7	(25,25)	4.94411	0.73853	0.15746
1	7	(25,26)	4.95718	0.68387	0.15649
1	7	(26,25)	4.93272	0.71091	0.09793
1	7	(26,26)	4.95432	0.65436	0.10095
1	9	(25,25)	4.82478	0.921	0.15724
1	9	(25,26)	4.83755	0.86584	0.15776
1	9	(26,25)	4.79132	0.88426	0.11612
1	9	(26,26)	4.81473	0.82837	0.12184
2	7	(25,25)	4.96934	0.86473	0.01732
2	7	(25,26)	4.98826	0.83966	0.01732
2	7	(26,25)	4.97558	0.78301	0.01732
2	7	(26,26)	4.98805	0.76064	0.01732
2	9	(25,25)	4.85373	0.96057	0.01732
2	9	(25,26)	4.86631	0.94578	0.01732
2	9	(26,25)	4.85275	0.85853	0.01732
2	9	(26,26)	4.85959	0.8466	0.01732
3	7	(25,25)	4.7894	0.80526	0.0855
3	7	(25,26)	4.90766	0.62121	0.04893
3	7	(26,25)	4.72684	0.84954	0.10222
3	7	(26,26)	4.82913	0.7035	0.05171
3	9	(25,25)	4.75257	0.94812	0.15999
3	9	(25,26)	4.85382	0.75199	0.098
3	9	(26,25)	4.69495	0.99634	0.15359
3	9	(26,26)	4.7795	0.84172	0.0987
4	7	(25,25)	4.86222	0.66136	0.19295
4	7	(25,26)	4.88697	0.62847	0.17919
4	7	(26,25)	4.80913	0.67229	0.15741
4	7	(26,26)	4.82516	0.65482	0.14189
4	9	(25,25)	4.76722	0.83137	0.17774
4	9	(25,26)	4.78572	0.80715	0.15244
4	9	(26,25)	4.72532	0.83442	0.15273
4	9	(26,26)	4.73824	0.81826	0.12612
5	7	(25,25)	4.74393	1.16586	0.08481
5	7	(25,26)	4.76468	1.09453	0.09385
5	7	(26,25)	4.75177	1.11631	0.08857
5	7	(26,26)	4.77499	1.05017	0.09886
5	9	(25,25)	4.62369	1.41415	0.02509
5	9	(25,26)	4.63422	1.34605	0.03397
5	9	(26,25)	4.63427	1.36947	0.02808
5	9	(26,26)	4.64675	1.30627	0.03778
6	7	(25,25)	5.07931	0.37814	0.13877
6	7	(25,26)	5.14171	0.31286	0.10161
6	7	(26,25)	5.11634	0.31783	0.09593
6	7	(26,26)	5.1789	0.27043	0.10044
6	9	(25,25)	4.97752	0.62436	0.11991
6	9	(25,26)	5.01796	0.5542	0.13044
6	9	(26,25)	5.00566	0.56704	0.11992
6	9	(26,26)	5.04808	0.49504	0.12892
7	7	(25,25)	4.87942	0.92416	0.03561
7	7	(25,26)	4.90284	0.88042	0.05461
7	7	(26,25)	4.86616	0.87325	0.01906
7	7	(26,26)	4.88696	0.8336	0.02451
7	9	(25,25)	4.74441	1.10841	0.01732
7	9	(25,26)	4.76104	1.08415	0.01793
7	9	(25,26)	4.74054	1.05178	0.01732
7	9	(26,26)	4.75756	1.02931	0.01732

Table A2. Cont.

Sampling Point	Height/m	Grid	Air Temperature (°C)	Heat Transfer Coefficient (m ² /s)	Wind Speed (m/s)
8	7	(25,25)	4.60172	1.38658	0.01732
8	7	(25,26)	4.59001	1.33089	0.01732
8	7	(26,25)	4.60631	1.34551	0.01732
8	7	(26,26)	4.5964	1.2865	0.01732
8	9	(25,25)	4.56218	1.51627	0.01732
8	9	(25,26)	4.55053	1.45792	0.01732
8	9	(26,25)	4.56434	1.48148	0.01732
8	9	(26,26)	4.5539	1.4205	0.01732

Table A3. The Raw Phenology Data of Reproductive Phenophases of Female *P. tomentosa*.

Sampling Point	Phenophase	Sample Tree 1			Sample Tree 2			Mean	SD
		Sample Branch 1	Sample Branch 2	Sample Branch 3	Sample Branch 1	Sample Branch 2	Sample Branch 3		
1	BBB	59	59	60	60	60	61	59.8	0.753
1	BF	65	66	66	66	66	67	66.0	0.632
1	FF	67	68	68	68	68	69	68.0	0.632
1	FS	70	70	70	70	70	71	70.2	0.408
1	BSD	94	95	95	95	95	96	95.0	0.632
1	ESD	103	104	104	104	105	104	104.0	0.632
1	DSD	9	9	9	9	10	8	9.0	0.632
2	BBB	59	58	59	59	59	59	58.8	0.408
2	BF	65	64	65	65	65	65	64.8	0.408
2	FF	67	66	67	67	67	67	66.8	0.408
2	FS	70	69	70	71	70	70	70.0	0.632
2	BSD	93	92	93	94	93	93	93.0	0.632
2	ESD	103	103	103	104	103	103	103.2	0.408
2	DSD	10	11	10	10	10	10	10.2	0.408
3	BBB	61	62	61	60	61	61	61.0	0.632
3	BF	68	69	68	67	68	68	68.0	0.632
3	FF	70	71	70	70	70	70	70.2	0.408
3	FS	72	73	72	72	72	72	72.2	0.408
3	BSD	95	96	95	94	95	95	95.0	0.632
3	ESD	103	103	103	102	103	103	102.8	0.408
3	DSD	8	7	8	8	8	8	7.8	0.408
4	BBB	61	61	60	61	61	62	61.0	0.632
4	BF	68	68	68	68	68	67	67.8	0.408
4	FF	69	69	69	69	69	69	69.0	0.000
4	FS	71	71	70	71	71	71	70.8	0.408
4	BSD	95	95	94	95	95	96	95.0	0.632
4	ESD	105	105	104	105	105	105	104.8	0.408
4	DSD	10	10	10	10	10	9	9.8	0.408
5	BBB	62	63	62	62	62	61	62.0	0.632
5	BF	68	69	68	68	68	67	68.0	0.632
5	FF	70	70	70	70	70	69	69.8	0.408
5	FS	72	72	73	72	72	71	72.0	0.632
5	BSD	95	96	95	95	95	95	95.2	0.408
5	ESD	102	103	102	102	102	101	102.0	0.632
5	DSD	7	7	7	7	7	6	6.8	0.408

Table A3. Cont.

Sampling Point	Phenophase	Sample Tree 1			Sample Tree 2			Mean	SD
		Sample Branch 1	Sample Branch 2	Sample Branch 3	Sample Branch 1	Sample Branch 2	Sample Branch 3		
6	BBB	58	58	57	58	59	58	58.0	0.632
6	BF	65	65	65	65	65	64	64.8	0.408
6	FF	67	67	67	67	67	66	66.8	0.408
6	FS	70	70	69	70	70	70	69.8	0.408
6	BSD	94	94	93	94	95	93	93.8	0.753
6	ESD	106	107	106	106	106	105	106.0	0.632
6	DSD	12	13	13	12	11	12	12.2	0.753
7	BBB	61	61	61	61	61	60	60.8	0.408
7	BF	67	66	67	67	66	67	66.7	0.516
7	FF	69	69	69	69	68	69	68.8	0.408
7	FS	71	71	71	71	70	71	70.8	0.408
7	BSD	94	94	94	94	93	93	93.7	0.516
7	ESD	102	103	102	102	102	101	102.0	0.632
7	DSD	8	9	8	8	9	8	8.3	0.516
8	BBB	63	62	63	64	63	63	63.0	0.632
8	BF	71	70	71	71	71	71	70.8	0.408
8	FF	72	72	73	72	72	72	72.2	0.408
8	FS	73	73	74	73	73	73	73.2	0.408
8	BSD	96	96	97	96	96	96	96.2	0.408
8	ESD	102	102	103	102	102	102	102.2	0.408
8	DSD	6	6	6	6	6	6	6.0	0.000

References

- Li, X.; Zhou, Y.; Asrar, G.R.; Mao, J.; Li, X.; Li, W. Response of vegetation phenology to urbanization in the conterminous United States. *Glob. Chang. Biol.* **2016**, *23*, 2818–2830. [CrossRef] [PubMed]
- Oke, T.R. The energetic basis of the urban heat island. *Q. J. R. Meteorol. Soc.* **1982**, *108*, 1–24. [CrossRef]
- Wohlfahrt, G.; Tomelleri, E.; Hammerle, A. The urban imprint on plant phenology. *Nat. Ecol. Evol.* **2019**, *3*, 1668–1674. [CrossRef] [PubMed]
- Zhou, D.; Zhao, S.; Zhang, L.; Liu, S. Remotely sensed assessment of urbanization effects on vegetation phenology in China's 32 major cities. *Remote Sens. Environ.* **2016**, *176*, 272–281. [CrossRef]
- Neil, K.; Wu, J. Effects of urbanization on plant flowering phenology: A review. *Urban Ecosyst.* **2006**, *9*, 243–257. [CrossRef]
- World Health Organization. *Regional Office for Europe. Phenology and Human Health: Allergic Disorders: Report on a WHO Meeting—Rome, Italy, 16–17 January 2003*; Report No. 108750; WHO Regional Office for Europe: Copenhagen, Denmark, 2003.
- Arnstein, T. Curse of the Catkins: A Brief History of Cottonwood Poplars in Beijing. 31 March 2019. Available online: <https://www.thebeijinger.com/blog/2014/04/17/curse-catkins-brief-history-cottonwood-poplars-beijing> (accessed on 31 December 2020).
- Wu, X.; Shi, T.; Chen, H.; Wang, H.; Sun, M.; Zhang, J. The microstructure and mechanical properties of poplar catkin fibers evaluated by atomic force microscope (AFM) and nanoindentation. *Forestry* **2019**, *10*, 938. [CrossRef]
- Columbus, J.T.; Wu, Z.; Raven, P.H.; Hong, D. Flora of China. *TAXON* **2008**, *57*, 682. [CrossRef]
- Hu, Y.; Ferguson, D.K.; Bera, S.; Li, C. Seed hairs of poplar trees as natural airborne pollen trap for allergenic pollen grains. *Grana* **2008**, *47*, 241–245. [CrossRef]
- Wan, X.; Gu, G.; Lei, M.; Zeng, W. Bioaccessibility of metals/metalloids in willow catkins collected in urban parks of Beijing and their health risks to human beings. *Sci. Total Environ.* **2020**, *717*, 137240. [CrossRef]
- Athar, P. Coronavirus bane for thousands of poplar trees in Kashmir. The local administration issues axing orders on female poplar trees fearing their cottony seeds may worsen COVID-19 symptoms. 2020. Available online: <https://www.natureasia.com/en/nindia/article/10.1038/nindia.2020.63> (accessed on 15 February 2021). [CrossRef]
- Bashaarat, M. Do 'Russian Poplar' Seeds Cause May Illness in Kashmir? The Fears, the Science. 13 May 2019. Available online: <https://indianexpress.com/article/explained/do-russian-poplar-seeds-cause-may-illness-in-kashmir-the-fears-the-science-5724268/> (accessed on 31 December 2020).
- Naqvi, S. Poplar Trees Creating Respiratory Problems in Abbottabad. 11 May 2019. Available online: <https://www.thenews.com.pk/print/469879-poplar-trees-creating-respiratory-problems-in-abbottabad> (accessed on 31 December 2020).
- Du, J. City Will Stop Planting Certain Trees to Curtail Catkins. 16 April 2019. Available online: <http://www.chinadaily.com.cn/a/201904/16/WS5cb52f56a3104842260b664e.html> (accessed on 31 December 2020).

16. Wong, L. Fluff Off: More than 300,000 Willow Trees to be Injected with Birth Control. 18 April 2018. Available online: http://www.timeoutbeijing.com/features/Blogs-Beijing_News/164015/Fluff-off-More-than-300,000-willow-trees-to-be-injected-with-birth-control.html (accessed on 31 December 2020).
17. Beijing Daily. The Flying-Catkin Season of Poplars and Willows in Beijing Will Begin This Week. 9 April 2020. Available online: http://bjrb.bjd.com.cn/html/2020-04/09/content_12455449.htm (accessed on 31 December 2020).
18. Jochner, S.C.; Sparks, T.H.; Estrella, N.; Menzel, A. The influence of altitude and urbanization on trends and mean dates in phenology (1980–2009). *Int. J. Biometeorol.* **2011**, *56*, 387–394. [[CrossRef](#)]
19. Parece, T.E.; Campbell, J.B. Intra-urban microclimate effects on phenology. *Urban Sci.* **2018**, *2*, 26. [[CrossRef](#)]
20. Qiu, T.; Song, C.; Li, J. Impacts of urbanization on vegetation phenology over the past three decades in Shanghai, China. *Remote Sens.* **2017**, *9*, 970. [[CrossRef](#)]
21. Zipper, S.C.; Schatz, J.; Singh, A.; Kucharik, C.J.; A Townsend, P.; Li, S.P.L. Urban heat island impacts on plant phenology: Intra-urban variability and response to land cover. *Environ. Res. Lett.* **2016**, *11*, 054023. [[CrossRef](#)]
22. Mimet, A.; Pellissier, V.; Quénot, H.; Aguejidad, R.; Dubreuil, V.; Rozé, F. Urbanisation induces early flowering: Evidence from *Platanus acerifolia* and *Prunus cerasus*. *Int. J. Biometeorol.* **2009**, *53*, 287–298. [[CrossRef](#)]
23. Amani-Beni, M.; Zhang, B.; Xie, G.-D.; Xu, J. Impact of urban park's tree, grass and waterbody on microclimate in hot summer days: A case study of Olympic Park in Beijing, China. *Urban For. Urban Green.* **2018**, *32*, 1–6. [[CrossRef](#)]
24. Yan, H. *The Effect of Urban Green Area on Urban Microclimate*; Beijing Forestry University: Beijing, China, 2014.
25. Pellis, A.; Laureysens, I.; Ceulemans, R. Genetic variation of the bud and leaf phenology of seventeen poplar clones in a short rotation coppice culture. *Plant Biol.* **2004**, *6*, 38–46. [[CrossRef](#)] [[PubMed](#)]
26. Tarayre, M.; Bowman, G.; Schermann-Legionnet, A.; Barat, M.; Atlan, A. Flowering phenology of *Ulex europaeus*: Ecological consequences of variation within and among populations. *Evol. Ecol.* **2007**, *21*, 395–409. [[CrossRef](#)]
27. Coder, K.D. *Tree Anatomy: Shoots and Growth Patterns*; Warnell School of Forestry & Natural Resources, University of Georgia, Outreach Publication: Athens, GA, USA, 2018; Available online: https://www.warnell.uga.edu/sites/default/files/publications/WSFNR-19-36_Coder.pdf#:~:text=Tree%20Anatomy:%20SHOOTS%20&%20GROWTH%20PATTERNS%20Tree%20shoots,,there%20are%20many%20meanings%20for%20the%20word%20%E2%80%9Cshoot.%E2%80%9D (accessed on 31 December 2020).
28. Stewart, I.D.; Oke, T.R. Local climate zones for urban temperature studies. *Bull. Am. Meteorol. Soc.* **2012**, *93*, 1879–1900. [[CrossRef](#)]
29. Yokobori, T.; Ohta, S. Effect of land cover on air temperatures involved in the development of an intra-urban heat island. *Clim. Res.* **2009**, *39*, 61–73. [[CrossRef](#)]
30. Wan, M.W.; Liu, X.Z. *Chinese Phenology Observation Method*; Science Press: Beijing, China, 1979.
31. Cornelius, C.; Petermeier, H.; Estrella, N.; Menzel, A. A comparison of methods to estimate seasonal phenological development from BBCH scale recording. *Int. J. Biometeorol.* **2011**, *55*, 867–877. [[CrossRef](#)] [[PubMed](#)]
32. Unwin, D.M. *Microclimate Measurement for Ecologists*; Academic Press: London, UK, 1980.
33. Bruse, M.; Fleer, H. Simulating surface-plant-air interactions inside urban environments with a three dimensional numerical model. *Environ. Model. Softw.* **1998**, *13*, 373–384. [[CrossRef](#)]
34. Liu, D.; Hu, S.; Liu, J. Contrasting the performance capabilities of urban radiation field between three microclimate simulation tools. *Build. Environ.* **2020**, *175*, 106789. [[CrossRef](#)]
35. Rui, L.; Buccolieri, R.; Gao, Z.; Gatto, E.; Ding, W. Study of the effect of green quantity and structure on thermal comfort and air quality in an urban-like residential district by ENVI-met modelling. *Build. Simul.* **2019**, *12*, 183–194. [[CrossRef](#)]
36. Salata, F.; Golasi, I.; Vollaro, R.D.L.; Vollaro, A.D.L. Urban microclimate and outdoor thermal comfort. A proper procedure to fit ENVI-met simulation outputs to experimental data. *Sustain. Cities Soc.* **2016**, *26*, 318–343. [[CrossRef](#)]
37. Sharmin, T.; Steemers, K.; Matzarakis, A. Microclimatic modelling in assessing the impact of urban geometry on urban thermal environment. *Sustain. Cities Soc.* **2017**, *34*, 293–308. [[CrossRef](#)]
38. Tselioui, A.; Tsiros, I.X. Modeling urban microclimate to ameliorate thermal sensation conditions in outdoor areas in Athens (Greece). *Build. Simul.* **2016**, *9*, 251–267. [[CrossRef](#)]
39. Tsoka, S.; Tsikaloudaki, A.; Theodosiou, T. Analyzing the ENVI-met microclimate model's performance and assessing cool materials and urban vegetation applications—A review. *Sustain. Cities Soc.* **2018**, *43*, 55–76. [[CrossRef](#)]
40. Zhao, Q.; Sailor, D.J.; Wentz, E.A. Impact of tree locations and arrangements on outdoor microclimates and human thermal comfort in an urban residential environment. *Urban For. Urban Green.* **2018**, *32*, 81–91. [[CrossRef](#)]
41. Penfield, S. Temperature perception and signal transduction in plants. *New Phytol.* **2008**, *179*, 615–628. [[CrossRef](#)]
42. Ng, E.; Chen, L.; Wang, Y.; Yuan, C. A study on the cooling effects of greening in a high-density city: An experience from Hong Kong. *Build. Environ.* **2012**, *47*, 256–271. [[CrossRef](#)]
43. Taleb, D.; Abu-Hijleh, B. Urban heat islands: Potential effect of organic and structured urban configurations on temperature variations in Dubai, UAE. *Renew. Energy* **2013**, *50*, 747–762. [[CrossRef](#)]
44. Ambrosini, D.; Galli, G.; Mancini, B.; Nardi, I.; Sfarra, S. Evaluating mitigation effects of urban heat islands in a historical small center with the ENVI-Met[®] climate model. *Sustainability* **2014**, *6*, 7013–7029. [[CrossRef](#)]
45. Middel, A.; Häb, K.; Brazel, A.J.; Martin, C.A.; Guhathakurta, S. Impact of urban form and design on mid-afternoon microclimate in Phoenix local climate zones. *Landsc. Urban Plan.* **2014**, *122*, 16–28. [[CrossRef](#)]

46. Chen, X.; Zhang, W.; Ren, S.; Lang, W.; Liang, B.; Liu, G. Temporal coherence of phenological and climatic rhythmicity in Beijing. *Int. J. Biometeorol.* **2017**, *61*, 1733–1748. [[CrossRef](#)] [[PubMed](#)]
47. Mudelsee, M. *Statistical Analysis of Climate Extremes*; Cambridge University Press (CUP): Cambridge, UK, 2020.
48. Xu, M.Z.; Ren, G.Y. Change in growing season over China: 1961. *J. Appl. Meteorol. Sci.* **2004**, *15*, 306–312. (In Chinese)
49. Erell, E.; Pearlmutter, D.; Williamson, T. *Urban Microclimate*; Routledge: London, UK, 2012.
50. Moreira, T.A.; Colmanetti, A.R.A.; Tibiriçá, C.B. Heat transfer coefficient: A review of measurement techniques. *J. Braz. Soc. Mech. Sci. Eng.* **2019**, *41*, 264. [[CrossRef](#)]
51. Duarte, D.H.; Shinzato, P.; Gusson, C.D.S.; Alves, C.A. The impact of vegetation on urban microclimate to counterbalance built density in a subtropical changing climate. *Urban Clim.* **2015**, *14*, 224–239. [[CrossRef](#)]
52. Yang, P.; Ren, G.; Liu, W. Spatial and temporal characteristics of Beijing urban heat island intensity. *J. Appl. Meteorol. Clim.* **2013**, *52*, 1803–1816. [[CrossRef](#)]
53. Willmott, C.J. Some comments on the evaluation of model performance. *Bull. Am. Meteorol. Soc.* **1982**, *63*, 1309–1313. [[CrossRef](#)]
54. Stunder, M.; Sethuraman, S. A statistical evaluation and comparison of coastal point source Dispersion Models. *Atmos. Environ.* **1967**, *20*, 301–315. [[CrossRef](#)]
55. Yang, X.; Zhao, L.; Bruse, M.; Meng, Q. Evaluation of a microclimate model for predicting the thermal behavior of different ground surfaces. *Build. Environ.* **2013**, *60*, 93–104. [[CrossRef](#)]
56. Hoerl, A.E.; Kennard, R.W. Ridge regression: Biased estimation for nonorthogonal problems. *Technometrics* **1970**, *12*, 55–67. [[CrossRef](#)]
57. McDonald, G.C. Ridge regression. *Wiley Interdiscip. Rev. Comput. Stat.* **2009**, *1*, 93–100. [[CrossRef](#)]
58. Dahlgren, J.P.; Zeipel, H.V.; Ehrlén, J. Variation in vegetative and flowering phenology in a forest herb caused by environmental heterogeneity. *Am. J. Bot.* **2007**, *94*, 1570–1576. [[CrossRef](#)] [[PubMed](#)]
59. Gehrman, F.; Hänninen, H.; Liu, C.; Saarinen, T. Phenological responses to small-scale spatial variation in snowmelt timing reveal compensatory and conservative strategies in subarctic-alpine plants. *Plant Ecol. Divers.* **2017**, *10*, 453–468. [[CrossRef](#)]
60. Jackson, M.T. Effects of microclimate on spring flowering phenology. *Ecology* **1966**, *47*, 407–415. [[CrossRef](#)]
61. Aono, Y.; Kazui, K. Phenological data series of cherry tree flowering in Kyoto, Japan, and its application to reconstruction of springtime temperatures since the 9th century. *Int. J. Clim.* **2008**, *28*, 905–914. [[CrossRef](#)]
62. Guo, L.; Dai, J.; Wang, M.; Xu, J.; Luedeling, E. Responses of spring phenology in temperate zone trees to climate warming: A case study of apricot flowering in China. *Agric. For. Meteorol.* **2015**, *201*, 1–7. [[CrossRef](#)]
63. Luo, Z.; Sun, O.J.; Ge, Q.; Xu, W.; Zheng, J. Phenological responses of plants to climate change in an urban environment. *Ecol. Res.* **2006**, *22*, 507–514. [[CrossRef](#)]
64. Tooke, F.; Battey, N.H. Temperate flowering phenology. *J. Exp. Bot.* **2010**, *61*, 2853–2862. [[CrossRef](#)]
65. Beaubien, E.G.; Freeland, H.J. Spring phenology trends in Alberta, Canada: Links to ocean temperature. *Int. J. Biometeorol.* **2000**, *44*, 53–59. [[CrossRef](#)] [[PubMed](#)]
66. Schwartz, M.D. *Phenology: An Integrative Environmental Science*, 2nd ed.; Springer: New York, NY, USA, 2013.
67. Thompson, R.; Clark, R.M. Spatio-temporal modelling and assessment of within-species phenological variability using thermal time methods. *Int. J. Biometeorol.* **2006**, *50*, 312–322. [[CrossRef](#)]
68. Memon, R.A.; Leung, D.Y.; Liu, C.-H. Effects of building aspect ratio and wind speed on air temperatures in urban-like street canyons. *Build. Environ.* **2010**, *45*, 176–188. [[CrossRef](#)]
69. Memon, R.A.; Leung, D.Y. Impacts of environmental factors on urban heating. *J. Environ. Sci.* **2010**, *22*, 1903–1909. [[CrossRef](#)]
70. Hagishima, A.; Tanimoto, J. Field measurements for estimating the convective heat transfer coefficient at building surfaces. *Build. Environ.* **2003**, *38*, 873–881. [[CrossRef](#)]
71. Eliasson, I.; Offerle, B.; Grimmond, C.; Lindqvist, S. Wind fields and turbulence statistics in an urban street canyon. *Atmos. Environ.* **2006**, *40*, 1–16. [[CrossRef](#)]
72. Giometto, M.; Christen, A.; Egli, P.; Schmid, M.; Tooke, R.; Coops, N.; Parlange, M. Effects of trees on mean wind, turbulence and momentum exchange within and above a real urban environment. *Adv. Water Resour.* **2017**, *106*, 154–168. [[CrossRef](#)]
73. Finn, G.; Straszewski, A.; Peterson, V. A general growth stage key for describing trees and woody plants. *Ann. Appl. Biol.* **2007**, *151*, 127–131. [[CrossRef](#)]
74. Acero, J.A.; Arrizabalaga, J. Evaluating the performance of ENVI-met model in diurnal cycles for different meteorological conditions. *Theor. Appl. Clim.* **2018**, *131*, 455–469. [[CrossRef](#)]
75. Song, B.-G.; Park, K.-H.; Jung, S.-G. Validation of ENVI-met model with in situ measurements considering spatial characteristics of land use types. *J. Korean Assoc. Geogr. Inf. Stud.* **2014**, *17*, 156–172. [[CrossRef](#)]
76. Konarska, J.; Holmer, B.; Lindberg, F.; Thorsson, S. Influence of vegetation and building geometry on the spatial variations of air temperature and cooling rates in a high-latitude city. *Int. J. Clim.* **2015**, *36*, 2379–2395. [[CrossRef](#)]